

LETTER

# Pressure-induced spin transition and evolution of the electronic excitations of $\text{FeBO}_3$ : Resonant inelastic x-ray scattering results

To cite this article: Jungho Kim *et al* 2014 *EPL* **108** 37001

View the [article online](#) for updates and enhancements.

## Related content

- [Crystal-field excitations in NiO under high pressure studied by resonant inelastic x-ray scattering](#)  
Simo Huotari, Laura Simonelli, Valentina M Giordano *et al*.
- [High-pressure studies with x-rays using diamond anvil cells](#)  
Guoyin Shen and Ho Kwang Mao
- [NiO as a test case for high resolution resonant inelastic soft x-ray scattering](#)  
G Ghiringhelli, M Matsubara, C Dallera *et al*.

## Recent citations

- [Weak Antiferromagnet Iron Borate  \$\text{FeBO}\_3\$ . Classical Object for Magnetism and the State of the Art](#)  
S. G. Ovchinnikov *et al*
- [Simulations of valence excited states in coordination complexes reached through hard X-ray scattering](#)  
Erik Källman *et al*
- [Solids, liquids, and gases under high pressure](#)  
Ho-Kwang Mao *et al*



**IOP | ebooks™**

Bringing together innovative digital publishing with leading authors from the global scientific community.

Start exploring the collection—download the first chapter of every title for free.

# Pressure-induced spin transition and evolution of the electronic excitations of FeBO<sub>3</sub>: Resonant inelastic x-ray scattering results

JUNGHO KIM<sup>1</sup>, VIKTOR V. STRUZHUKIN<sup>2(a)</sup>, SERGEY G. OVCHINNIKOV<sup>3,4</sup>, YU. ORLOV<sup>3</sup>, YU. SHVYD'KO<sup>1</sup>, M. H. UPTON<sup>1</sup>, D. CASA<sup>1</sup>, ALEXANDER G. GAVRILIUK<sup>2,5,6(b)</sup> and S. V. SINOGEIKIN<sup>7</sup>

<sup>1</sup> *Advanced Photon Source, Argonne National Laboratory - Argonne, IL 60439, USA*

<sup>2</sup> *Geophysical Laboratory, Carnegie Institution of Washington - 5251 Broad Branch Road NW, Washington DC 20015, USA*

<sup>3</sup> *L. V. Kirensky Institute of Physics, Siberian Branch of Russian Academy of Sciences - Krasnoyarsk 660036, Russia*

<sup>4</sup> *Siberian Federal University - 79 Svobodny Prospect, Krasnoyarsk 660041, Russia*

<sup>5</sup> *Institute for Nuclear Research, Russian Academy of Sciences - Troitsk, Moscow 142190, Russia*

<sup>6</sup> *Institute of Crystallography, Russian Academy of Sciences - 119333, Leninskii pr-t 59, Moscow, Russia*

<sup>7</sup> *HPCAT, Carnegie Institution of Washington - 9700 South Cass Avenue, Argonne, IL 60439, USA*

received on 16 October 2014; accepted by S. Savrasov on 18 October 2014

published online 31 October 2014

PACS 71.27.+a – Strongly correlated electron systems; heavy fermions

PACS 62.50.-p – High-pressure effects in solids and liquids

PACS 78.70.Ck – X-ray scattering

**Abstract** – A high-pressure resonant inelastic x-ray scattering (RIXS) of FeBO<sub>3</sub> at the Fe *K* pre-edge has been carried out to study the evolution of electronic excitations through the pressure-induced spin transition. Systematic peak shifts with insignificant peak width change are observed with increasing pressure in the high-spin state. An electronic transition occurs in tandem with the high-spin to low-spin transition, observed as the emergence of multiple new low-energy peaks in the spectra. The energy gap is reduced due to these low-energy peaks, not a peak width broadening. The observed electronic excitations are associated with *dd* excitations, which are calculated using a full-multiplet theory. We consider changes in crystal-field splitting and covalency to explain the observed peak shifts in the high-spin state. The new peaks that emerge upon the high- to low-spin transition are compared with *dd* excitations for the low-spin configuration.



Copyright © EPLA, 2014

**Introduction.** – Pressure-induced spin transitions from high-spin (HS) to low-spin (LS) states are fundamentally related to central problems in condensed-matter physics and geophysics [1,2] such as a metal-insulator transition (MIT) [3–8] and seismological anomalies in the Earth's lower mantle [9,10]. Difficulties in understanding the underlying mechanism arise because there are simultaneously evolving and intertwined energy scales under pressure such as the crystal-field splitting and the band width [1,3–5,11]. Useful insights can be obtained by finding a model system in which one of the energy scales plays the primary role and by measuring its electronic excitation spectrum by an appropriate spectroscopic tool.

Iron borate FeBO<sub>3</sub> is an antiferromagnetic Mott insulator with a gap of 2.9 eV and Néel temperature of 348 K

at ambient pressure [12,13]. The Fe<sup>3+</sup> ions centered in the O<sub>6</sub><sup>2-</sup> octahedron are in the high-spin configuration, resulting in a local spin  $S = 5/2$ . Above 46 GPa, the local moment becomes smaller (low-spin state with  $S = 1/2$ ), and the energy gap decreases to 0.8 eV, as found by the Mössbauer spectroscopy [14] and optical absorbance [13], respectively. The low-spin state is isostructural with the high-spin state [15]. Band structure calculations suggested that *3d* orbitals in FeBO<sub>3</sub> are weakly hybridized with ligands because of a very strong hybridization inside the BO<sub>3</sub> group [13,16,17]. Hence, the competition between the crystal-field splitting and Hund's intra-atomic exchange energy is important in the spin transition, making FeBO<sub>3</sub> a good candidate system where the spin transition is driven by an increase of the crystal-field splitting under pressure. A multielectron model based on the local density approximation combined with a generalized tight-binding approach (LDA+GTB) showed that the Hubbard

(a) E-mail: vstruzhkin@carnegiescience.edu

(b) E-mail: gavriliuk@mail.ru

energy gap (energy cost of moving an electron from site to site) is smaller in the low-spin state than in the high-spin state, which was interpreted to explain the reduced energy gap in the low-spin state [13,18].

Attempts to measure electronic excitation spectra up to a few eV at high pressure have been stymied heretofore by the technical difficulties inherent in measuring a sample held at high pressure in a diamond anvil cell (DAC). Hard x-ray resonant inelastic x-ray scattering (RIXS), a bulk-sensitive and element-specific spectroscopic probe of valence excitations, can be used to measure such excitations in the DAC environment and provide a wealth of information on a few eV electronic excitations [2,19]. Fe  $K$  edge RIXS measurements on  $\text{FeBO}_3$  at ambient pressure revealed a number of excitation peaks in the energy loss range 3–12 eV [20]. Those observed excitation peaks were attributed to inter-site electronic excitations between  $\text{Fe}^{3+}$  and  $\text{O}_6^{2-}$  (*i.e.*, charge-transfer excitation) or between adjacent  $\text{Fe}^{3+}$  ions (*i.e.*, Mott-Hubbard excitations).

**Experimental procedure.** – In this work, we report a study of electronic excitations of  $\text{FeBO}_3$  at high pressure by RIXS at the Fe  $K$  pre-edge, focusing on how the electronic structure evolves in the HS state as pressure increases and on how the electronic structure is modified in the LS state. The 180 meV energy resolution and good counting statistics are crucial to resolve fine structures in the spectra, which were not clear in the past high-pressure RIXS measurements on NiO [21], CoO [2], and  $\text{La}_{5/3}\text{Sr}_{1/3}\text{NiO}_4$  [22]. In this measurement, the spin transition was also measured by  $K\beta_{1,3}$  emission and pre-edge absorption spectra simultaneously with the RIXS measurement. In the HS state, excitation peaks show systematic shifts with insignificant peak width change. Above  $P = 53$  GPa (LS state), the excitation spectrum undergoes a drastic change. Multiple lower-energy peaks appear below 5 eV, resulting in a reduced gap of 1 eV. The excitation peaks of the RIXS at the Fe  $K$  pre-edge have been attributed to  $dd$  excitations.  $dd$  excitations are calculated by using a full-multiplet, single-cluster approach including the covalence effect and are used to account for the peak shifts in the HS state, the gap decrease, and multiple features in the LS state.

RIXS spectra at room temperature were measured using the MERIX instrument at the 30-ID beamline of the advanced photon source (APS). The beam was focused to  $40(\text{H}) \times 20(\text{V}) \mu\text{m}^2$ . Details in the RIXS setup are described in ref. [20]. Here, the horizontal scattering geometry is used, where the incident photon polarization is parallel to the scattering plane (see fig. 1). The scattering angle  $2\theta$  was held at  $90^\circ$  where the elastic scattering cross-section is strongly suppressed. Each spectrum was measured by scanning the scattered photon energy  $E_f$  with the incident photon energy  $E_i$  fixed, and plotted as a function of the energy loss,  $\omega \equiv E_i - E_f$ . The energy resolution was 180 meV.

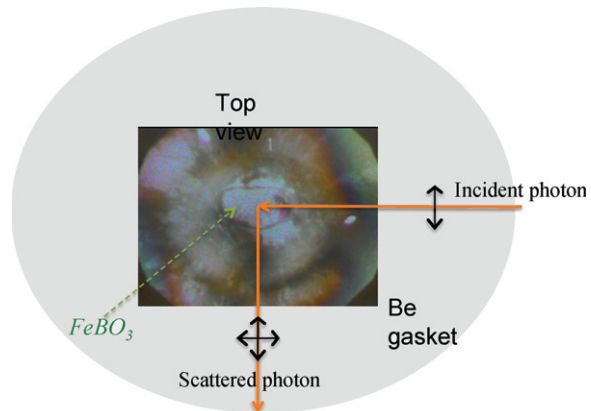


Fig. 1: (Colour on-line) Scattering geometry in the RIXS experiment. The  $\text{FeBO}_3$  single crystal was loaded into the 50 mm diameter hole of a Be gasket with an inset made from boron nitride powder mixed with epoxy. Both incident and scattered photons go through the Be gasket.

A  $\text{FeBO}_3$  single crystal was loaded into the 50  $\mu\text{m}$  diameter hole of a Be gasket with an inset made from boron nitride powder mixed with epoxy as shown in fig. 1. In the first measurement, the pressure ( $P$ ) was measured using the off-line Raman system at beamlines 13 (GSECARS) and 16 (HPCAT) at the APS, and pressure gradients across the sample were estimated from the edge of the first-order Raman peak of the diamond anvil [23]. In the second measurement, a small piston-cylinder, membrane-driven DAC with enlarged side openings was used for the *in situ* pressure control [24]. The membrane drive of the cell will be described elsewhere [25]. The pressure was measured with an *in situ* Ruby fluorescence system. The two independent measurements yielded nearly identical results.

RIXS spectra were collected through the Be gasket as shown in fig. 1 [2,26,27]. We will refer to the pre-edge RIXS when the incident photon energy is tuned to the energy of the Fe  $K$  pre-edge absorption. The pre-edge RIXS is used for the following reasons. The pre-edge RIXS signal is strong even at  $2\theta = 90^\circ$ , where the main-edge RIXS signal is strongly reduced [20]. The probing depth is larger than the main-edge region because of a weak pre-edge absorption. The resonance energy can be precisely tuned because the pre-edge absorption consists of well-defined peaks, contrary to the broad main-edge absorption. The energy resolution at the pre-edge is better because  $E_f$  is closer to the analyzer back-scattering energy. Because  $3d$  orbitals are directly involved in the scattering process, excitations between  $3d$  orbitals can be observed [28,29].

Two spectroscopic measurements were performed simultaneously with the RIXS measurements. The  $K\beta_{1,3}$  emission spectrum was measured with  $E_i = 7.2$  keV. Figure 2(a) shows the emission spectra for  $P = 24$  and 44 GPa. The lower  $E_f$  satellite structures around 7.045 eV originate from the  $3p$ - $3d$  exchange interaction in the HS configuration. In the LS configuration, it is well known

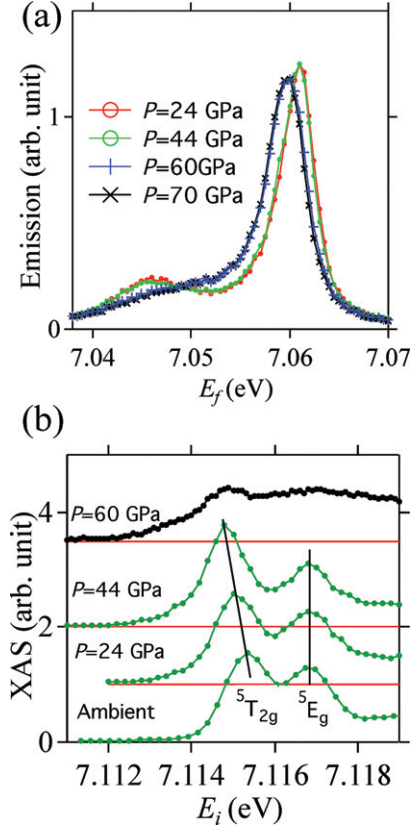


Fig. 2: (Colour on-line) (a)  $K\beta_{1,3}$  emission spectra. At 60 and 70 GPa, the lower  $E_f$  satellite structure disappears, indicating that the system is in the LS state. (b) Pre-edge XAS. As  $P$  increases, the energy difference between  ${}^5T_{2g}$  and  ${}^5E_g$  increases. At 60 GPa, there are no longer well-defined peaks.

that the satellite structure becomes weakened and the main peak energy is lowered due to the transferred spectral weight from the satellite structure [2,30]. The spectra for  $P = 60$  and 70 GPa clearly show these spectral changes.

Second, the pre-edge x-ray absorption spectroscopy (XAS) spectrum was measured using the main peak of the  $K\beta_{1,3}$  emission [2,30]. In fig. 2(b), two well-defined peaks are identified for the ambient,  $P = 24$ , and 44 GPa. Two peaks can be assigned to  ${}^5T_{2g}$  and  ${}^5E_g$  in the order of increasing energy. As  $P$  increases, the energy difference between these two peaks increases. This increase is due to the increase in the crystal-field splitting under pressure. Note that the pre-edge peak energy difference is related to the crystal-field splitting in the excited state ( $3d^6$ ), which is smaller than the crystal-field splitting in the ground state ( $3d^5$ ) [31]. At  $P = 60$  GPa, these two peaks are no longer well defined and the pre-edge XAS consists of broad structures. In the LS configuration, the pre-edge XAS consists of  ${}^1A_1$ ,  ${}^3T_1$ ,  ${}^3T_2$ ,  ${}^1T_1$ , and  ${}^1T_2$  in the order of increasing energy, resulting in a much broader spectral feature as can be found in ref. [31]. Two measurements indicate that FeBO<sub>3</sub> is in the HS state below 44 GPa and in the LS state above 60 GPa.

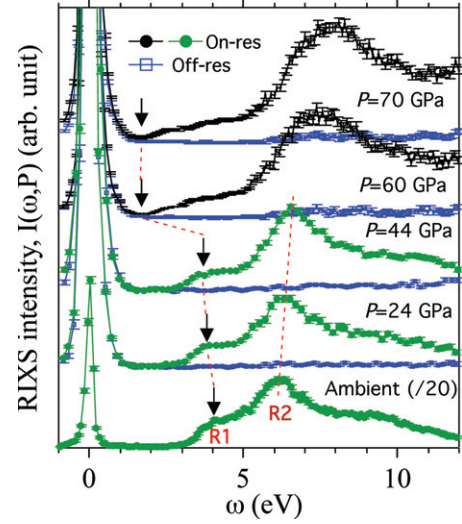


Fig. 3: (Colour on-line) RIXS spectra for the HS state ( $P =$  ambient, 24, and 44 GPa) and the LS state (60 and 70 GPa) taken with the on-resonance conditions. RIXS spectra taken with the off-resonance conditions are also shown. Systematic peak shifts are seen for the HS state. A drastic spectral difference is seen between HS and LS states. In particular, the gap is reduced from 3 eV to 1 eV.

**Results and discussion.** – The main experimental results of RIXS spectra for the HS state (the ambient,  $P = 24$ , and 44 GPa) and the LS state ( $P = 60$  and 70 GPa) are shown in fig. 3. The on-resonance (On-res) RIXS spectra were measured by tuning  $E_i$  to the  ${}^5T_{2g}$  pre-edge XAS peak energy (7.1153 keV at the ambient pressure, 7.115 keV at 24 GPa, and 7.1148 keV for 44, 60, and 70 GPa) while  $E_i = 7.112$  eV was used for all off-resonance (Off-res) spectra<sup>1</sup>. The ambient pressure spectrum is divided by 20 for comparison with the RIXS spectra measured with the pressure cell. Stronger elastic intensities at  $\omega = 0$  for the pressure cell data are due to other sources for the elastic scattering, such as the Be gasket.

In fig. 3, the RIXS spectra for the HS states show two well-defined peaks at 4 and 6 eV (indicated by R1 and R2, respectively) and a broad feature up to 12 eV. The R1 and R2 peaks do not show any noticeable broadening under pressure. On the other hand, the R1 peak slightly shifts towards a lower energy at a rate of  $-0.0034$  eV/GPa. On the other hand, the R2 peak shifts towards a higher energy at a rate of  $0.0134$  eV/GPa. The results are summarized in fig. 5(a). The pressure dependence of the relative peak shift of R1 and R2,  $0.0168$  eV/GPa, is close to that of the crystal-field splitting,  $0.018$  eV/GPa, from the optical study [13,18].

In the LS states ( $P = 60$  and 70 GPa), the R1 and R2 peaks are no longer well defined. RIXS spectra consist of multiple peaks below 5 eV and a broad strong structure at 8 eV. In order to subtract the elastic signals and resolve

<sup>1</sup>In the case of  $P = 60$  and 70 GPa,  $E_i = 7.1147$  keV was used for the on-resonance RIXS spectra.

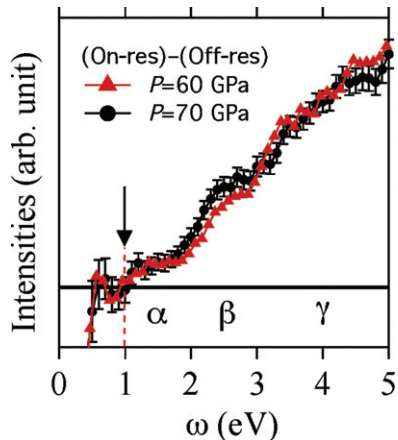


Fig. 4: (Colour on-line) Difference data of the On-res and the Off-res. RIXS spectra for the LS state (60 and 70 GPa) were taken to subtract the elastic signals and resolve low-intensity peaks at low  $\omega$ . Low-energy spectra consist of multiple structures;  $\alpha$ ,  $\beta$  and  $\gamma$ .

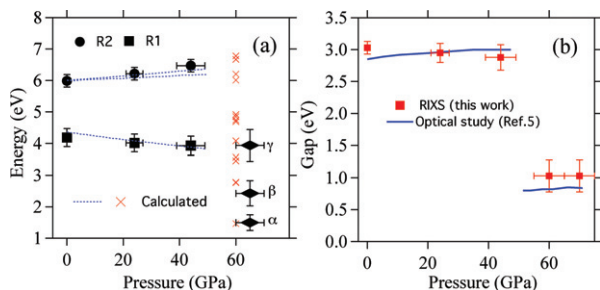


Fig. 5: (Colour on-line) (a) Summary of the observed peak energies and the calculations of Mott-Hubbard excitation. (b) Energy gap values as a function of pressure. The result from the optical study [13] is drawn.

low-intensity peaks at low  $\omega$ , we obtain the difference data of the on-resonance and the off-resonance spectra. In fig. 4, those difference spectra for  $P = 60$  and  $70$  GPa are displayed, focusing on the multiple peaks below  $\omega = 5$  eV. For both spectra, we can identify two peaks at  $1.5$  and  $2.5$  eV and one broad peak centered at  $4$  eV, which are indicated as  $\alpha$ ,  $\beta$  and  $\gamma$ , respectively. The energy gap, *i.e.*, the onset energy of the inelastic intensity is reduced due to these low-energy peaks. The energy gaps are summarized in fig. 5(b). The result from the optical study is drawn as a solid line for a comparison [13]. Energy gap values derived from two different spectroscopy data sets are in good agreement with each other.

The process of the pre-edge RIXS is that the incident photon promotes a  $1s$  core electron into an empty  $3d$  valence state, and subsequently an electron from the valence band decays, annihilating the  $1s$  core hole. This type of RIXS is often called “direct” RIXS and allows probing the valence and conduction states directly [19]. In cases of NiO and copper oxides,  $dd$  excitations in a single site (*i.e.*, on-site  $dd$  excitations) were observed by the pre-edge RIXS [28,29,32]. In the high-pressure study of

NiO,  $dd$  excitations between adjacent sites (*i.e.*, Mott-Hubbard excitations) were associated to one of the observed excitation peaks [21]. These excitations between  $d$  orbitals are not suppressed at the 90-degree horizontal scattering geometry. The ambient pressure RIXS study on FeBO<sub>3</sub> showed that the excitations in the pre-edge RIXS are distinctive from the charge-transfer excitations in the main-edge RIXS and the incident photon polarization, momentum transfer and temperature dependences could be consistently explained in terms of Mott-Hubbard excitations [20]. Note that there is no spin-allowed on-site  $dd$  excitation in the case of the high-spin Fe<sup>3+</sup>, which can be probed by the pre-edge RIXS [19,20].

Here, we used the full-multiplet calculations with inclusions of the crystal-field splitting and the covalency to calculate the Mott-Hubbard excitation energies [33].

Mott-Hubbard excitation energy is defined by  $[E(d^6; \Gamma_6) + E(d^4; \Gamma_4) - 2E(d^5; \Gamma_5)]$ , where  $\Gamma_n$  denotes each electron configuration symmetry. The multielectron band structure calculations for the infinite lattice by the LDA + DMFT [34,35] and the LDA + GTB [36,37] methods can provide a full account for the inter-atomic hopping. In a spectroscopic study of a Mott insulator, a multiplet calculation based on a model Hamiltonian is widely used to explain the excitation spectrum [38–42]. FeBO<sub>3</sub> has the small inter-atomic hopping which would result in a band width of the order of the RIXS spectral line width. The local full-multiplet calculation, which corresponds to a zeroth-order approximation of the inter-atomic hopping, can be regarded as a reasonable approach to the calculation of Mott-Hubbard excitations in FeBO<sub>3</sub>.

Here, we consider all possible  $dd$  excitations in the framework of the full-multiplet, single-cluster model and compare calculated energies of  $dd$  excitations with the peak positions and shifts of RIXS excitation spectra<sup>2</sup> S<sup>10</sup>. In this calculation, the influence of the FeO<sub>6</sub> octahedral distortion is assumed to be insignificant. The  $3d$  spin-orbit coupling and inter-atomic exchange on the excitation energy calculations are not considered. The multiplet energy is described by Racah parameters  $A$ ,  $B$ ,  $C$ . The Racah parameters are assumed to be pressure independent. The crystal-field splitting parameter,  $\Delta$ , is subject to change due to the lattice contraction and set to be  $1.57 + vP$  eV, where  $v = 0.018$  eV/GPa [13,18]. Covalency arises from the hopping of electrons between the oxygen and the iron. Within the single-cluster calculations, the covalency is the only term which admixes  $d^n$  and  $d^{n+1}\underline{L}$ , where  $\underline{L}$  denotes a ligand hole. Covalency is included in the calculation, by the exact diagonalization of the FeO<sub>6</sub> cluster with multi-electron molecular orbitals with proper orbital symmetry and spin value constructed in ref. [43]. The charge-transfer energy ( $D = E(d^6\underline{L}) - E(d^5)$ ) is set to be  $3.8$  eV [20].

<sup>2</sup>Our comparison of the excitation energies between the Kanamori approximation and the full-multiplet theory showed almost no difference for the high-spin state while a large difference was found for the low-spin state.

Hopping amplitudes,  $t_{pd}$  and  $t_{pp}$ , are assumed to be linearly dependent on  $P$ . We derived  $t_{pd}(P) = 0.7 + 0.008P$  and  $t_{pp}(P) = 0.5 + 0.008P$  eV.

The lowest Mott-Hubbard excitation in the HS state has the energy  $\varepsilon_{E1} = A + 14B + 7C - \Delta$ . Higher excitations are  $\varepsilon_{E2} = \varepsilon_{E2'} = \varepsilon_{E1} + \Delta$  and  $\varepsilon_{E3} = \varepsilon_{E1} + 2\Delta$ . When the parameters for the ambient pressure ( $A = 1.9$ ,  $B = 0.084$ ,  $C = 0.39$  and  $\Delta = 1.57$  eV) from the optical study [13] are used,  $\varepsilon_{E1} = 4.236$  eV and  $\varepsilon_{E2} = \varepsilon_{E2'} = 5.806$  eV are obtained for the ambient pressure. We could associate the R1 ( $\sim 4.18$  eV) peak with the  $E1$  excitation and the R2 ( $\sim 5.99$  eV) peak with the  $E2$  and  $E2'$  excitations. The degeneracy of the  $E2$  and  $E2'$  excitations is lifted at higher pressure by the covalency. The  $E2$  and  $E2'$  peaks shift towards higher energy, while the  $E1$  peak shifts towards lower energy.

In the LS state, the lowest Mott-Hubbard excitation is given by  $\varepsilon_{L1} = A + 9B - 7C$ . Many higher-energy Mott-Hubbard excitations exist in the LS state formed by a number of Mott-Hubbard excitations with different excited  $d^4$  and  $d^6$  terms with spin- and orbital-allowed matrix elements. Mott-Hubbard excitations are at 1.466, 2.767, 2.767, 2.783, 3.458, 3.57, 4.084, 4.084, 4.695, 4.743, 4.743, 4.855, 4.855, 4.92, 6.012, 6.205, 6.205, 6.671, 6.783, and 8.133 eV in the order of increasing energy. A number of the Mott-Hubbard excitations, which constitute the  $\varepsilon_{L4}$  and  $\varepsilon_{L5}$  peaks, belong to the energy region of the strong broad feature around 8 eV. But it is unlikely that those Mott-Hubbard excitations are exceptionally enhanced in the RIXS process. Considering its much broader width and stronger intensity, some other contributions besides the  $dd$  excitations, such as the  $K_{2,5}$  emission, seem to exist in the small gap state of the LS. In a LS Fe<sup>3+</sup>, spin-allowed on-site  $dd$  excitations exist and also calculated from the full-multiplet theory. The lowest on-site  $dd$  excitation energy is proportional to the crystal-field splitting, which is 2.65 eV at 60 GPa, assuming the pressure dependence of 0.018 eV/GPa. On-site  $dd$  excitations are at 1.836, 1.92, 2.256, 2.676, 3.096, 3.516, and 4.602 eV in the order of increasing energy. Because of different intra- and inter-orbitals Coulomb interactions in different electron configurations, the lowest on-site  $dd$  excitation energy is smaller than the crystal-field splitting.

Figure 5(a) shows the calculation results with the experimental data. The pressure dependence of the Mott-Hubbard excitation energies in the high-spin state reasonably reproduces the observed pressure dependence of the R1 and R2 peaks. The downward shift of the lowest Mott-Hubbard excitation is due to both increases in the crystal-field splitting and the covalency, while the upward shifts of the second Mott-Hubbard excitations are due to the increase in the covalency. In the case of the low-spin state, Mott-Hubbard excitations densely exist in the energy region of the  $\gamma$  peak (3–5 eV). On the other hand, the  $\alpha$  and  $\beta$  peaks have a single Mott-Hubbard excitation in the corresponding energy region. Particularly, the lowest Mott-Hubbard excitation is well separated from

higher excitations and matches its energy (1.47 eV) with the  $\alpha$  peak. In the low-spin Fe<sup>3+</sup> state, a number of on-site  $dd$  excitations are spin allowed in the pre-edge RIXS. The lowest on-site  $dd$  excitation energy is proportional to the crystal-field splitting, which is 2.65 eV at 60 GPa assuming a pressure dependence of 0.018 eV/GPa. So, the  $\alpha$  peak can be assigned to the Mott-Hubbard excitation, implying a Mott insulating state in the low-spin state.

The RIXS spectra in fig. 3 show that the peak widths do not change much when the system approaches the spin transition. For example, the slope of the leading edge of the R1 peak shows no noticeable change as pressure increases. With our assignment of the observed peaks to the Mott-Hubbard excitations, this observation indicates that the electronic structure of FeBO<sub>3</sub> evolves under pressure without much change in the  $3d$  band width. This observation supports the results from the band structure calculations [13,16,17], including the generalized gradient approximation (GGA) +  $U$  [33];  $3d$  orbitals in FeBO<sub>3</sub> are weakly hybridized with ligands because of a very strong hybridization inside the BO<sub>3</sub> group. So, FeBO<sub>3</sub> is a system in which one can see the effects of the increase of the crystal-field splitting on the electronic structure evolution without a complication from the band width change. The local stability of the high-spin state of Fe<sup>3+</sup> is no longer sustained at high pressure when the increase of the crystal-field splitting exceeds Hund's exchange energy. When the local spin arrangement of Fe<sup>3+</sup> is changed from the high-spin to the low-spin, more Mott-Hubbard excitations arise at lower energies, which are interpreted to explain the reduced energy gap [13,18]. A similar system may be found in various Fe<sup>3+</sup> compounds such as GdFe<sub>3</sub>(BO<sub>3</sub>)<sub>4</sub>, BiFeO<sub>3</sub> [44,45], and Fe<sup>3+</sup> bearing silicate perovskite in the Earth's lower mantle [46]. In this type of system, lattice contraction under pressure naturally leads to the increase of the crystal-field splitting. Unlike highly hybridized  $d^5$  systems such as TM mono-oxides [4,47] and hematite [5], the band width broadening does not come into play. The covalency, *i.e.*, the hybridization of the  $3d$  with the surrounding oxygen ligands, changes because of a shortened distance or a bonding symmetry change. In our interpretation, it is suggested that the covalency change affects the energies of the electronic excitations together with the crystal-field splitting, although the covalency does not play a decisive role in the driving mechanism of the spin transition in FeBO<sub>3</sub> because it does not lead to any electronic and structural instabilities.

**Summary.** – High-resolution RIXS at the Fe  $K$  pre-edge provides spectroscopic information about the evolution of the electronic structure through the spin state transition, which is otherwise difficult or impossible to obtain. We suggest that FeBO<sub>3</sub> is a good benchmark system for the study of the spin transition in a Mott insulator driven by an increase of the crystal-field splitting. We consider all possible  $dd$  excitations in the framework of the full-multiplet, single-cluster model and compare the

calculated energies of *dd* excitations with the observed peaks of RIXS excitation spectra. The observed peak shifts in the high-spin state are consistent with the energy shifts of the Mott-Hubbard excitations by changes in the crystal-field splitting and the covalency. The lowest Mott-Hubbard excitation matches its energy with the experimentally observed peak, which causes the small energy gap of the low-spin state. We suggest that the Hubbard correlation among Fe 3*d* electrons dictates the nature of the low-spin insulating state of FeBO<sub>3</sub>. The demonstrated RIXS technique could be applied to a multitude of questions surrounding spin transitions of iron in the Earth's mantle materials, and may clarify their relation to optical properties, heat transfer, and conductivity of the mantle.

\* \* \*

High-pressure work was supported by DOE under Contract No. DE-FG02-02ER45955. The use of the Advanced Photon Source at the Argonne National Laboratory was supported by the U.S. DOE under Contract No. DE-AC02-06CH11357. SGO and YUO acknowledge the President of Russia Grants NSh-1044.2012.2 and MK-1168.2012.2, the Presidium of the Russian Academy of Sciences Program 2, RFFI Grants 12-02-90410 and 12-02-31543, FCP GK-P891, and the Siberian Federal University Grant F11. AGG acknowledges support from the Russian Foundation for Basic Research grants 14-02-00483 and 15-02-03770 from RAS programs "Strongly correlated electron systems", "Elementary particle physics, fundamental nuclear physics and nuclear technologies".

## REFERENCES

- [1] COHEN R. E., MAZIN I. I. and ISAAK D. G., *Science*, **275** (1997) 654.
- [2] RUEFF J.-P. and SHUKLA A., *Rev. Mod. Phys.*, **82** (2010) 847.
- [3] WERNER P. and MILLIS A. J., *Phys. Rev. Lett.*, **99** (2007) 126405.
- [4] MATTILA A. *et al.*, *Phys. Rev. Lett.*, **98** (2007) 196404.
- [5] KUNES J. *et al.*, *Phys. Rev. Lett.*, **102** (2009) 146402.
- [6] GAVRILIUK A. G., LYUBUTIN I. S. and STRUZHUKIN V. V., *JETP Lett.*, **86** (2007) 532.
- [7] GAVRILIUK A. G., TROJAN I. A. and STRUZHUKIN V. V., *Phys. Rev. Lett.*, **109** (2012) 086402.
- [8] GAVRILIUK A. G. *et al.*, *Phys. Rev. B*, **77** (2008) 155112.
- [9] NOMURA R. *et al.*, *Nature*, **473** (2011) 199.
- [10] SPEZIALE S. *et al.*, *Proc. Natl. Acad. Sci. U.S.A.*, **102** (2005) 17918.
- [11] KUNES J. and KRAPEK V., *Phys. Rev. Lett.*, **106** (2011) 256401.
- [12] EDELMAN I. S. *et al.*, *Sov. Phys.: Solid State*, **14** (1973) 2442.
- [13] GAVRILIUK A. G. *et al.*, *JETP Lett.*, **99** (2004) 566.
- [14] TROYAN I. A. *et al.*, *JETP Lett.*, **74** (2001) 24.
- [15] GAVRILIUK A. G. *et al.*, *JETP Lett.*, **75** (2002) 23.
- [16] POSTNIKOV A. V. *et al.*, *Phys. Rev. B*, **50** (1994) 14849.
- [17] IVANOVA N. B. *et al.*, *JETP*, **94** (2002) 299.
- [18] OVCHINNIKOV S. G. *et al.*, *Phys. Met. Metallogr.*, **99** (2005) 93.
- [19] AMENT L. J. P. *et al.*, *Rev. Mod. Phys.*, **83** (2011) 705.
- [20] KIM J., SHVYD'KO Y. and OVCHINNIKOV S. G., *Phys. Rev. B*, **83** (2011) 235109.
- [21] SHUKLA A. *et al.*, *Phys. Rev. B*, **67** (2003) 081101.
- [22] SIMONELLI L. *et al.*, *Phys. Rev. B*, **84** (2011) 195140.
- [23] AKAHAMA Y. and KAWAMURA H., *J. Appl. Phys.*, **100** (2006) 043516.
- [24] GAVRILIUK A. G., MIRONOVICH A. A. and STRUZHUKIN V. V., *Rev. Sci. Instrum.*, **80** (2009) 043906.
- [25] SINOGEIKIN S., in preparation.
- [26] ZENG Q.-S. *et al.*, *Phys. Rev. Lett.*, **104** (2010) 105702.
- [27] LIN J. F. *et al.*, *Am. Mineral.*, **95** (2010) 1125.
- [28] HUOTARI S. *et al.*, *Phys. Rev. B*, **78** (2008) 041102(R).
- [29] KIM J. *et al.*, *Phys. Rev. B*, **81** (2010) 073109.
- [30] VANKO G. *et al.*, *J. Phys. Chem. B*, **110** (2006) 11647.
- [31] WESTRE T. E. *et al.*, *J. Am. Chem. Soc.*, **119** (1997) 6297.
- [32] VAN VEENENDAAL M. *et al.*, *Phys. Rev. B*, **83** (2011) 045101.
- [33] SHANG S. *et al.*, *Appl. Phys. Lett.*, **91** (2007) 253115.
- [34] ANISIMOV V. I. *et al.*, *J. Phys.: Condens. Matter*, **9** (1997) 7359.
- [35] HELD K. *et al.*, *Int. J. Mod. Phys. B*, **15** (2001) 2611.
- [36] KORSHUNOV M. M. *et al.*, *Phys. Rev. B*, **72** (2005) 165104.
- [37] SHNEYDER E. I. *et al.*, *JETP Lett.*, **96** (2012) 349.
- [38] CHEN C.-C. *et al.*, *Phys. Rev. Lett.*, **105** (2010) 177401.
- [39] KOVALEVA N. N. *et al.*, *Phys. Rev. Lett.*, **93** (2004) 147204.
- [40] OLES A. M. *et al.*, *Phys. Rev. B*, **72** (2005) 214431.
- [41] GÖSSLING A. *et al.*, *Phys. Rev. B*, **77** (2008) 035109.
- [42] KOTANI A. and SHIN S., *Rev. Mod. Phys.*, **73** (2001) 203.
- [43] ORLOV Y. S. and OVCHINNIKOV S. G., *JETP*, **109** (2009) 322.
- [44] LYUBUTIN I. S. *et al.*, *Phys. Rev. B*, **79** (2009) 085125.
- [45] LYUBUTIN I. S. and GAVRILIUK A. G., *Phys.-Usp.*, **52** (2009) 989.
- [46] FROST D. J. *et al.*, *Nature*, **428** (2004) 409.
- [47] KUNES J. *et al.*, *Nat. Mater.*, **7** (2008) 198.